Sarah K. Scholten, James D. Anstie, Nicolas Bourbeau Hébert, Richard T. White, Jérôme Genest, and Andre N. Luiten

Complex direct comb spectroscopy with a virtually imaged phased array

Optics Letters, 2016; 41(6):1277-1280

Complex direct comb spectroscopy with a virtually imaged phased array

SARAH K. SCHOLTEN[1,*], JAMES D. ANSTIE[1], NICOLAS BOURBEAU HÉBERT[2], RICHARD T. WHITE[1], JÉRÔME GENEST[2], AND ANDRE N. LUITEN[1]

[1] Institute for Photonics and Advanced Sensing, School of Physical Sciences, The University of Adelaide, Adelaide SA 5005, Australia
[2] Centre d'Optique, photonique et laser, Université Laval, Québec, GIV 0A6, Canada
[*] Corresponding author: sarah.scholten@adelaide.edu.au

Compiled March 1, 2016

We demonstrate a simple interferometric technique to directly measure the complex optical transmittance over a large spectral range using a frequency-comb spectrometer based on a virtually imaged phased array (VIPA). A Michelson interferometer encodes the phase deviations induced by a sample contained in one of its arms into an interferogram image. When combined with an additional image taken from each arm separately, along with a frequency-calibration image, this allows full reconstruction of the sample's optical transfer function. We demonstrate the technique with a vapor cell containing $H^{13}C^{14}N$, producing transmittance and phase spectra spanning 2.9 THz ($\sim$23 nm) with $\sim$1 GHz resolution.

OCIS codes: *(140.4050) Mode-locked lasers; (300.1030) Spectroscopy, absorption; (300.6390) Spectroscopy, molecular; (120.5050) Phase measurement; (110.5100) Phased-array imaging systems.*

http://dx.doi.org/10.1364/ao.XX.XXXXXX

Optical frequency combs have been a revolutionary development for spectroscopy, allowing fast measurements, broad spectral coverage, dense spectral sampling and absolute frequency accuracy [1]. Further, in contrast to many other broadband sources, frequency combs are also spatially and temporally coherent, making comb sources useful for measurements of both a sample's amplitude and phase response. In this letter we exploit these properties to make direct, high quality measurements of the complex transmittance of a molecular sample.

The magnitude of the optical response of some sample, whether transmittance, absorbance or reflectance, is the most commonly reported spectroscopic measurement. It is much easier to obtain than the phase response, and it is conventionally held that the Kramers-Kronig relations [2, 3] provide a means to derive both the real and imaginary components of the complex transfer function from the magnitude measurement. However, this is only formally true for causal, linear and time-invariant systems that have the property of minimal phase [4]. For non-minimal phase systems, the spectral phase cannot be retrieved from the amplitude spectrum, and thus a distinct measurement of the phase response is required to determine the complete optical transfer function. There are numerous optical measurements that can benefit from the separate acquisition of phase including: dispersion measurements of optical fibers and components [5], reflectivity characterization of optical thin films [6], detailed lineshape perturbation analysis [7] and the probing of certain cavity configurations, most notably micro-resonators [8, 9].

Interferometric spectrometers, such as Fourier-transform [10, 11], dual-comb [12] and frequency modulated continuous wave (FMCW) spectrometers [5, 13, 14] can be configured to yield complex measurements; however, spectrometers based on spatial dispersion are in general simpler and more robust. Gohle *et al.* [15] have achieved phase measurements using a Fabry-Perot cavity based discriminator but, to our knowledge, high-quality direct phase measurements with a spatially resolved spectrometer have yet to be demonstrated.

In this letter, we demonstrate a technique suitable for simultaneously measuring both amplitude and phase spectra using a comb in conjunction with a virtually imaged phased array (VIPA) spectrometer [16, 17]. The $2\nu_3$ vibrational overtone band of $H^{13}C^{14}N$ is used as a minimal-phase optical system to demonstrate accurate phase retrieval. Measurement of the full optical transfer function is achieved with the addition of a Michelson interferometer. One arm of the interferometer is actively length stabilized such that a $\lambda/4$ offset from the path matched condition is maintained. Working at this point ensures that all comb modes experience essentially the same phase shift due to the length mismatch (to within a small linear factor) and leaves the phase shift due to molecular interaction simply encoded within three camera images.

The experimental setup is shown in Fig. 1. The frequency comb (Menlo Systems FC1500) spans $\sim$1500–1600 nm. Its carrier-envelope-offset frequency (f_{CEO}) is locked to a cesium beam clock (Datum CsIII), while the comb repetition rate (f_{RR}) of $\sim$250 MHz is stabilized by locking the nearest comb mode to a cavity-stabilized reference laser (NKT Koheras Boostik E15). The comb is combined with the reference laser, which acts as a marker for optical frequency calibration. The light then follows one of two paths: either it travels through a stabilized low finesse ($\sim$200) Fabry-Perot (FP) cavity (grey dashed path), or it bypasses the cavity (solid path) and enters the rest of the experiment. The

cavity, with a free spectral range (FSR) of $35 \times f_{RR} = 8.75\,\text{GHz}$ is set to transmit every 35$^{\text{th}}$ comb mode and is used to calibrate the optical frequency axis. The beam is then sent, *via* a four-port 50:50 coupler and Glan-Thompson polarizer (to ensure identical beam polarizations), into a wedged beam splitter (WBS) that feeds the two arms of a Michelson interferometer.

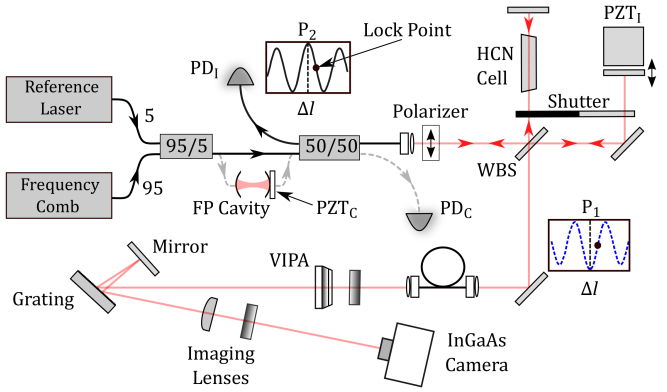

Fig. 1. A simplified schematic of the experiment. Also shown is the power at the two output ports of the interferometer, P_1 and P_2, as a function of length detuning (Δl) from the global interference maximum at P_2 at the path-matched condition.

One arm of the interferometer (sample path) contains a 50 mm-long cell of $H^{13}C^{14}N$ at 100 ± 10 Torr (Wavelength References HCN-13-100) at room temperature ($22.5 \pm 1^\circ$ C). The second arm (reference path) controls the interference condition between the two arms of the interferometer *via* a mirror on a piezoelectric (PZT) stage (PZT_I). After recombination, light from the retro-reflected output port (P_2) is directed back to a photodetector (PD_I) for use in locking the interferometer. Light from the other output port (P_1) is directed through an optical fiber to enforce beam overlap, before being line-focused into the AR-coated input window of a VIPA etalon (Light Machinery). The VIPA is a specialized étalon with a free spectral range (FSR) of ~50 GHz and a finesse of ~100 that disperses the comb light vertically as a function of wavelength [18]. To avoid frequency ambiguity [19], the VIPA is used in combination with a 600-lines/mm diffraction grating, oriented to disperse the light horizontally. The grating is double-passed to provide higher angular resolution [20]. The resulting beam is imaged on an InGaAs camera (Xenics Xeva-1.7-320) with a ~2.9 THz (~23 nm) spectral range in the horizontal direction and just over one VIPA FSR in the vertical direction.

Retrieval of the transmittance and phase data may be understood by considering the recombination of a single comb mode at the imaged output of the interferometer (P_1). For a light field of form: $E_0 \exp\left[i\left(\omega t + \phi\right)\right]$, where E_0 is the electric field amplitude, ϕ is the optical phase and ω is the angular optical frequency, feeding the interferometer through an ideal 50:50 beam splitter. In this case, the magnitude of the interference (P_1) is:

$$P_1 = E_1^2 + E_2^2 - 2E_1E_2\cos\left(\Delta\phi - \frac{2\pi\Delta l}{\lambda}\right), \tag{1}$$

where $E_1 = \alpha E_0/\sqrt{4}$, α^2 is the attenuation from a double pass through the sample; $E_2 = E_0/\sqrt{4}$; Δl is the change in round-trip optical path length of the sample arm with respect to the reference arm; λ is the wavelength and $\Delta\phi$ is the phase shift from a double pass through the sample. $\Delta\phi$ is thus:

$$\Delta\phi = \arccos\left(\frac{E_1^2 + E_2^2 - P_1}{2E_1E_2}\right) + \frac{2\pi\Delta l}{\lambda}. \tag{2}$$

In order to obtain the largest unambiguous phase range and highest phase sensitivity, the interferometer should be tuned such that $\Delta l = \lambda/4$. If we now consider the full ensemble of comb modes then this length tuning can only be exact for one central wavelength (λ_c). If the interferometer is locked such that it satisfies $\Delta l = \lambda_c/4$, an additional term dependent on detuning from λ_c is required to fully describe the phase shift of an individual comb mode. When working with optical frequency combs it is more natural to use optical frequency, so we introduce $\Delta\nu = (\nu - \nu_c)$ with $\nu_c = c/\lambda_c$. Expressed in terms of frequency, and with the additional detuning-dependent term, the equation for the sample phase shift becomes:

$$\Delta\phi\left(\nu\right) = \arcsin\left(\frac{E_1^2 + E_2^2 - P_1}{2E_1E_2}\right) + \Phi\left(\Delta\nu\right), \tag{3}$$

where $\Delta\phi\left(\nu\right)$ is the phase shift of an individual comb mode due to interaction with the sample and $\Phi\left(\Delta\nu\right) = \left[\pi/\left(2\nu_c\right)\right]\Delta\nu$ is the additional term due to the mode's deviation from ν_c, which dominates linear dispersion effects from other optical components. Note that Eqs. 1–3 imply that deviation from a 50:50 split ratio does not impact phase recovery.

We now describe the process for deriving the complex transmittance. First, we measure two separate VIPA images from the sample and reference paths alone (by blocking the alternative path) which yield E_1^2 and E_2^2 respectively. We then measure an interferogram image when operating at $\Delta l = \lambda_c/4$ to find P_1. The transmittance (T) is found from $T = E_1^2/E_2^2 = \alpha^2$ and the phase from Eq. 3.

As previously stated, to obtain a high quality interferogram image, the interferometer length imbalance must be tuned and stabilized such that $\Delta l = \lambda_c/4$. This is achieved by measuring the retro-reflected interferometer output port (P_2 on Fig. 1) using a photodetector (PD_I), which is used to lock the interferometer at half of its global maximum, as shown in Fig. 2. The error signal is then passed to a proportional-integral (PI) filter, the output of which is passed *via* a piezo controller to the PZT actuator (PZT_I) to stabilize the reference-arm length.

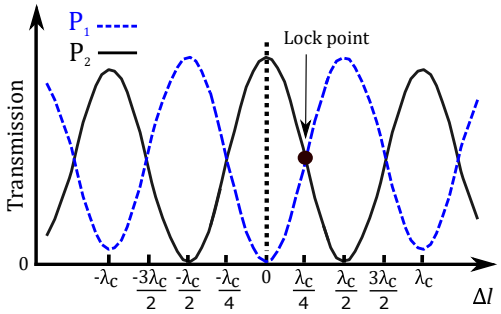

Fig. 2. The output of both ports (P_1 and P_2 in Fig. 1) of the interferometer as a function of length detuning (Δl) from the path-matched condition (dashed vertical line).

With the interferometer length locked, the interferogram image is recorded (Fig. 3(a)). The interferometer lock is then disabled, and the reference and sample paths are alternately blocked, recording a sample and reference image, respectively.

The interferogram image is acquired with 1 ms of integration time, while the sample and reference images are integrated for 2 ms in order to make best use of the available camera intensity resolution. In the current configuration, switching between the three image states is done manually, but this can easily be automated to reduce acquisition times to ∼100 ms.

In order to ensure frequency accuracy of the measurement, a final frequency calibration image is acquired by imaging the decimated, fully resolved, comb that results from passing through the FP cavity. This image is taken with the sample path blocked, and with the FP cavity length stabilized such that it transmits only the subset of comb-modes containing the mode nearest to the reference laser, as well as the reference itself. This point is found by scanning the cavity length and monitoring the photodetector (PD_C), stopping at the appropriate local maximum. The cavity length is dithered around this point and the demodulated transmission signal is used as an error signal to lock the cavity length [21]. This delivers a decimated version of the comb with every 35^{th} mode transmitted through the cavity as shown in Fig. 3(b). The VIPA resolution is sufficient to fully resolve the decimated comb and thus allows us to identify and assign a frequency to every imaged comb mode. This in turn allows us to make a high-quality calibration of the frequency at every location on the images.

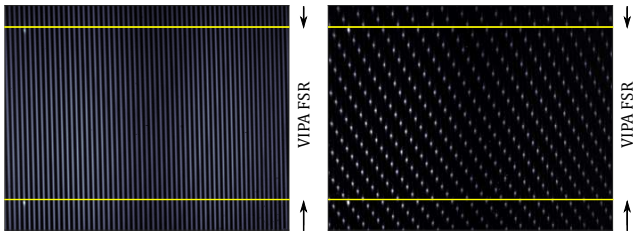

Fig. 3. Left: a typical raw interferogram. The two brightest spots correspond to the reference laser and the yellow horizontal lines mark out one VIPA FSR containing unique spectral data. The horizontal separation of adjacent bright vertical stripes is also one VIPA FSR [19]. Right: raw cavity-decimated image showing fully resolved comb modes.

The reference, sample and interferogram images contain a series of near vertical stripes (see Fig. 3(a)), with each stripe encoding just over one VIPA FSR of spectral information limited by the VIPA resolution (∼1 GHz). The vertical stripes are spaced horizontally by one VIPA FSR (∼50 GHz). The use of the double-pass grating confers sufficient horizontal resolution to ensure that these features are well separated, minimizing potential cross-talk between adjacent stripes. It is possible to calculate the transmittance and (uncorrected) phase directly from the image data, shown in Fig. 4, which may be useful for optical fingerprinting applications where a detailed understanding of the spectra is not so important. For more quantitative applications we have developed a process to reconstruct the underlying spectra in a more robust way.

The reference image is used as a key to extract the spectral information from all three images. The horizontal cross-section of each stripe within the reference image is essentially Gaussian, with each pixel contributing a signal proportional to the amount of optical power falling within its borders. By averaging a large number of these cross-sections, we can find an approximation to

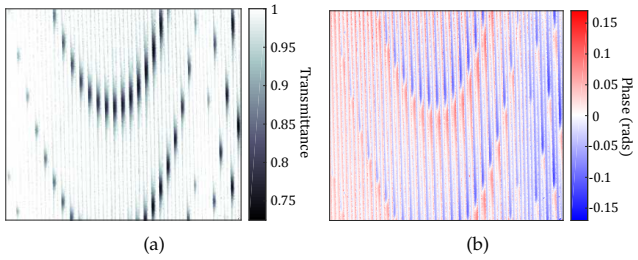

Fig. 4. Two-dimensional molecular fingerprints for absorption (left) and phase (right). The effects of the phase ramp are evident in the phase data.

the underlying Gaussian intensity profile (point spread function). We use this width approximation, along with an estimate of the center position, to construct a set of matched filters that mimic the observed cross-sections. We then calculate the sum of the pixel-by-pixel products between each cross-section and its corresponding filter, producing a weighted sum that maximizes the available signal-to-noise ratio and suppresses any residual cross-talk between adjacent stripes to well below the noise floor of the measurement. Applying this process to the entire image allows efficient extraction of the spectral data, with one data point per row per stripe. The set of matched filters derived from the reference image is also used to extract spectral information from the sample and interferogram images.

As mentioned previously and shown in Fig. 3(b), an image of the decimated comb and reference laser is used to generate an optical frequency axis for the spectral data extracted from each image. Measurements of the wavelength of the reference laser (HighFinesse WS/7, accurate to ∼10 MHz), comb repetition rate and carrier-envelope-offset frequency, allow for each imaged mode to be identified [21]. Least-squares fitting of the identified modes to a mapping function determines the relationship between optical frequency and position on the image.

Finally, the transmittance ($T = E_1^2/E_2^2$) and phase (Eq. 3) are calculated with E_1^2, E_2^2 and P_1 supplied by the spectral data determined from the sample, reference and interferogram images respectively. The central frequency (ν_c) for the phase correction can be estimated by choosing ν_c such that the off-resonance phase is zero; in this case, ∼176.2 THz. For non-minimal phase systems, determination of ν_c is more difficult, leading to uncertainties in phase offset and slope, governed by Eq. 3. In this case ν_c may be determined, for example, by using a CW laser of known λ to lock the path length imbalance and thus set ν_c.

Fig. 5 shows the measured transmittance and phase for a single measurement of the P1–P24 and R0–R4 lines of the $2\nu_3$ vibrational overtone band of $H^{13}C^{14}N$ and Fig. 6 shows a close-up of the P8 and P9 features. Also visible in these spectra are a series of smaller hot-band features [23]. The recorded transmittance spectrum has a signal-to-noise ratio of ∼500 (with sensitivity of ∼1000 ppm at 1 atm). It corresponds well to a model based on previous high-resolution measurements of $H^{13}C^{14}N$ [21, 22], represented by the solid red curve, with the optical path length through the sample and a linear background correction as the only free parameters. The phase spectrum exhibits a slightly reduced signal-to-noise ratio (phase sensitivity of ∼1 mrad), primarily due to non-linearity of the camera. It also corresponds well to the expected phase response (blue solid curve) modelled by a Faddeeva function approximation to the complex Voigt profile applied to the high-resolution data. Instrumental broadening

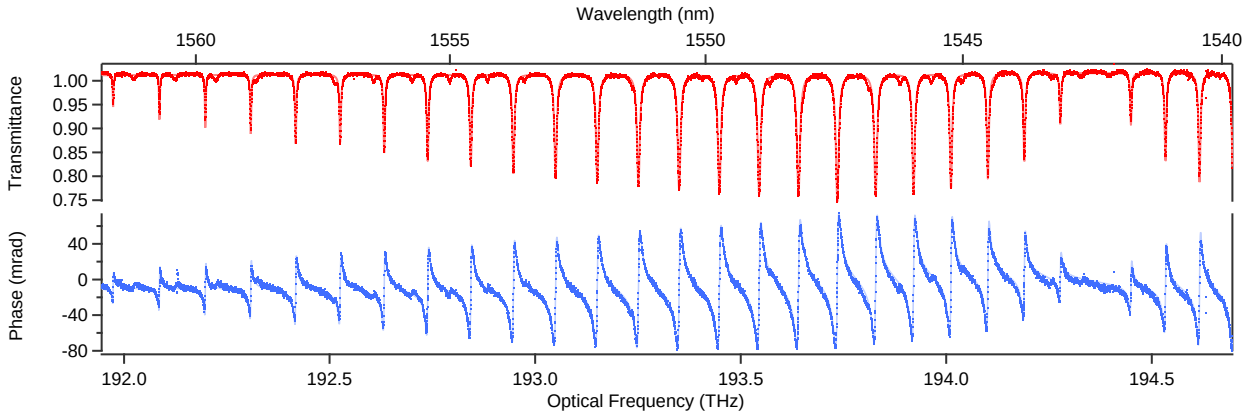

Fig. 5. Extracted transmittance and phase spectra for the P1–P24 and R0–R3 features of $H^{13}C^{14}N$. The solid lines show the modelled transmittance (red) and phase (blue) based on a previous high-resolution absorption measurement [21, 22]. Small (unmodelled) hot-band features can also be seen in both the transmission and phase data.

of the measured features with respect to the high-resolution measurement is due to the resolution limit of the VIPA.

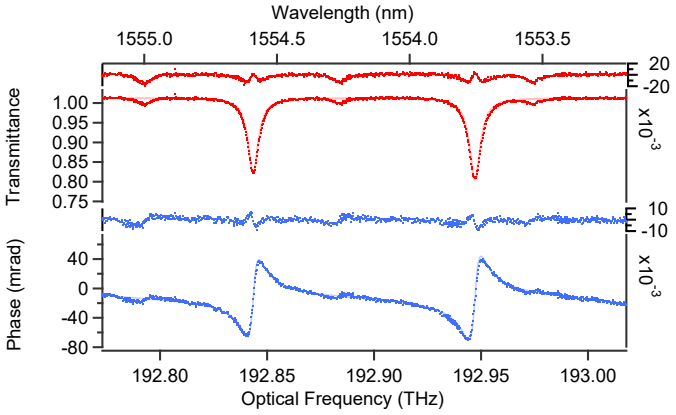

Fig. 6. Close-up of the P8 and P9 features of $H^{13}C^{14}N$ of Fig. 5. Smaller (unmodelled) hot-band features and instrumental broadening can be seen in both spectra and residuals.

In conclusion, we have demonstrated a direct interferometric measurement of the complex transmittance of $H^{13}C^{14}N$ using a VIPA-based frequency comb spectrometer. Though powerful in its current form, this technique is best suited to phase variations of < 1 rad, which can be overcome by locking to a range of path imbalances to unambiguously determine relative phase. It is also currently limited by the VIPA resolution, which can be improved by fully resolving individual comb modes and thus taking advantage of the intrinsic frequency accuracy of the stabilized optical frequency comb. This technique demonstrates a simple, fast, accurate and practical way to directly extract broadband amplitude and phase spectra, with potential application to a diverse range of optical systems.

ACKNOWLEDGMENTS

The authors would like to thank the Australian Research Council (ARC) for supporting this research through the LP120200605 and LP140100674 Linkage Project grants. The authors also wish to acknowledge the Government of South Australia for providing financial support through a Catalyst Research Grant and the Premiers Science and Research Fund.

REFERENCES

1. F. Adler, M. J. Thorpe, K. C. Cossel, and J. Ye, Annu. Rev. Anal. Chem. **3**, 175–205 (2010).
2. R. de L. Kronig, J. Opt. Soc. Am. **12**, 547–557 (1926).
3. H. A. Kramers, Atti Cong. Intern. Fisica, (Transactions of Volta Centenary Congress) pp. 545–557 (1927).
4. J. Bechhoefer, Am. J. Phys. **79** (2011).
5. T. Ahn, Y. Jung, K. Oh, and D. Kim, Opt. Express **13**, 10040–100048 (2005).
6. P. Grosse and V. Offermann, Appl. Phys. A **52**, 138–144 (1991).
7. J. Wang, P. Ehlers, I. Silander, and O. Axner, J. Opt. Soc. Am. B **28**, 2390–2401 (2011).
8. H. Bergeron, J. R. Carrier, V. Michaud-Belleau, J. Roy, J. Genest, and C. Allen, Phys. Rev. A. **87**, 063835 (2013).
9. V. Michaud-Belleau, J. Roy, S. Potvin, J. Carrier, L. Verret, M. Charlebois, J. Genest, and C. Allen, Opt. Express **20**, 3066–3075 (2012).
10. J. Birch, Mikrochimica Acta **93**, 105–122 (1987).
11. J. Mandon, G. Guelachvili, and N. Picqué, Nat. Photonics **3**, 99–102 (2009).
12. I. Coddington, W. C. Swann, and N. R. Newbury, Phys. Rev. Lett., **100**, 013902 (2008).
13. A. Cygan, P. Wcisło, S. Wójtewicz, P. Masłowski, J. T. Hodges, R. Ciuryło, and D. Lisak, Opt. Express **23**, 14472 (2015).
14. A. Foltynowicz, F. M. Schmidt, W. Ma, and O. Axner, Appl. Phys. B **92**, 313–326 (2008).
15. C. Gohle, B. Stein, A. Schliesser, T. Udem, and T. W. Hänsch, Phys. Rev. Lett. **99**, 263902 (2007).
16. L. Nugent-Glandorf, T. Neely, F. Adler, A. J. Fleisher, K. C. Cossel, B. Bjork, T. Dinneen, and S. A. Diddams, Opt. Lett. **37**, 3285–3287 (2012).
17. L. Nugent-Glandorf, F. R. Giorgetta, and S. A. Diddams, Appl. Phys. B **119**, 327–228 (2015).
18. M. Shirasaki, Opt. Lett. **21**, 366–368 (1996).
19. S. A. Diddams, L. Hollberg, and V. Mebele, Nature **445**, 627–630 (2007).
20. D. Derickson, *Fibre Optic Test and Measurement* (Prentice Hall, 1998), 1st ed.
21. N. B. Hébert, S. K. Scholten, R. T. White, J. Genest, A. N. Luiten, and J. D. Anstie, Opt. Express **23**, 13991–14001 (2015).
22. S. L. Gilbert, W. C. Swann, and C. Wang, NIST special publication **260**, 137 (2005).
23. H. Sasada and K. Yamada, Appl. Opt. **29**, 3535–3547 (1990).

REFERENCES

1. F. Adler, M. J. Thorpe, K. C. Cossel, and J. Ye, "Cavity-enhanced Direct Frequency Comb Spectroscopy: Technology and Applications," Annu. Rev. Anal. Chem. **3**, 175–205 (2010).
2. R. de L. Kronig, "On the theory of the dispersion of X-rays," J. Opt. Soc. Am. **12**, 547–557 (1926).
3. H. A. Kramers, "La diffusion de la lumiére par les atomes," Atti Cong. Intern. Fisica, (Transactions of Volta Centenary Congress) pp. 545–557 (1927).
4. J. Bechhoefer, "Kramers-Kronig, Bode, and the meaning of zero," Am. J. Phys. **79** (2011).
5. T. Ahn, Y. Jung, K. Oh, and D. Kim, "Optical frequency-domain chromatic dispersion measurement method for higher-order modes in an optical fibre," Opt. Express **13**, 10040–100048 (2005).
6. P. Grosse and V. Offermann, "Analysis of reflectance data using the Kramers-Kronig relations," Appl. Phys. A **52**, 138–144 (1991).
7. J. Wang, P. Ehlers, I. Silander, and O. Axner, "Dicke narrowing in the dispersion mode of detection and in noise-immune cavity-enhanced optical heterodyne molecular spectroscopy - theory and experimental verification," J. Opt. Soc. Am. B **28**, 2390–2401 (2011).
8. H. Bergeron, J. R. Carrier, V. Michaud-Belleau, J. Roy, J. Genest, and C. Allen, "Optical impulse response of silica microspheres: Complementary approach to whispering-gallery-mode analysis," Phys. Rev. A. **87**, 063835 (2013).
9. V. Michaud-Belleau, J. Roy, S. Potvin, J. Carrier, L. Verret, M. Charlebois, J. Genest, and C. Allen, "Whispering gallery mode sensing with a dual frequency comb probe," Opt. Express **20**, 3066–3075 (2012).
10. J. Birch, "Dispersive Fourier transform spectroscopy," Mikrochimica Acta **93**, 105–122 (1987).
11. J. Mandon, G. Guelachvili, and N. Picqué, "Fourier trasform spectroscopy with a laser frequency comb," Nat. Photonics **3**, 99–102 (2009).
12. I. Coddington, W. C. Swann, and N. R. Newbury, "Coherent multiheterodyne spectroscopy using stabilized optical frequency combs," Phys. Rev. Lett. **100**, 013902 (2008).
13. A. Cygan, P. Wcisło, S. Wójtewicz, P. Masłowski, J. T. Hodges, R. Ciuryło, and D. Lisak, "One-dimensional frequency-based spectroscopy," Opt. Express **23**, 14472 (2015).
14. A. Foltynowicz, F. M. Schmidt, W. Ma, and O. Axner, "Noise-immune cavity-enhanced optical heterodyne molecular spectroscopy: Current status and future potential," Appl. Phys. B **92**, 313–326 (2008).
15. C. Gohle, B. Stein, A. Schliesser, T. Udem, and T. W. Hänsch, "Frequency comb vernier spectroscopy for broadband, high-resolution, high-sensitivity absorption and dispersion spectra," Phys. Rev. Lett. **99**, 263902 (2007).
16. L. Nugent-Glandorf, T. Neely, F. Adler, A. J. Fleisher, K. C. Cossel, B. Bjork, T. Dinneen, and S. A. Diddams, "Mid-infrared virtually imaged phased array spectrometer for rapid and broadband trace gas detection," Opt. Lett. **37**, 3285–3287 (2012).
17. L. Nugent-Glandorf, F. R. Giorgetta, and S. A. Diddams, "Open-air, broad-bandwidth trace gas sensing with a mid-infrared optical frequency comb," Appl. Phys. B **119**, 327–228 (2015).
18. M. Shirasaki, "Large angular dispersion by a virtually imaged phased array and its application to a wavelength demultiplexer," Opt. Lett. **21**, 366–368 (1996).
19. S. A. Diddams, L. Hollberg, and V. Mebele, "Molecular fingerprinting with the resolved modes of a femtosecond laser frequency comb," Nature **445**, 627–630 (2007).
20. D. Derickson, *Fibre Optic Test and Measurement* (Prentice Hall, 1998), 1st ed.
21. N. B. Hébert, S. K. Scholten, R. T. White, J. Genest, A. N. Luiten, and J. D. Anstie, "A quantitative mode-resolved frequency comb spectrometer," Opt. Express **23**, 13991–14001 (2015).
22. S. L. Gilbert, W. C. Swann, and C. Wang, "Hydrogen cyanide H13C14N absorption reference for 1530 nm to 1565 nm wavelength calibration–SRM 2519a," NIST special publication **260**, 137 (2005).
23. H. Sasada and K. Yamada, "Calibration lines of HCN in the 1.5-μm region," Appl. Opt. **29**, 3535–3547 (1990).